

# Charcoal obtained from cherry bones in different carbonisation atmospheres

A. Venegas-Gomez<sup>a,\*</sup>, M. Gomez Corzo<sup>b,\*\*</sup>

<sup>a</sup>Department of Physics and SUPA, University of Strathclyde, Glasgow G4 0NG, UK

<sup>b</sup>Departamento de Química Inorgánica, Facultad de Ciencias, Universidad of Extremadura, Badajoz 07071, Spain

## Abstract

The exploitation of using agro-industrial residues as the cherry bone to produce charcoal and activated carbon is very relevant nowadays due to the high demand of these materials. This work describes the methods to prepare charcoal from cherry bones (*H*) using final heating temperature of 600°C, with or without the application of an equal flow of nitrogen or air. The isothermal time has been of 2 hours, an adequate time to study carbonisation by varying the atmosphere. The charcoal obtained has the appropriate characteristics as precursors of activated carbon. Of the three samples prepared in different atmospheres (6002N, N6002 and A6002N), the third is an activated carbon. In order to study the effects of the atmosphere during the heat treatment of *H*, the yield, chemical composition and structure, and the pore structure of the samples, are studied in this work.

**Keywords:** charcoal, cherry bones, carbonisation

## 1. Introduction

Agricultural, forestry and industrial residues of lignocellulosic nature (where the main components are cellulose and lignin, as in wood and fruit bones) are suitable for the production of charcoal and activated carbon. The process of heating organic materials in the absence of air is called pyrolysis or carbonisation. Generally the term pyrolysis is used when this process focuses on obtaining the gases and oils that are produced, and carbonisation when the process is directed towards the resulting solid product (charcoal). The carbonisation of the raw material is usually a prior step in the manufacture of the activated carbon, which results from an additional treatment with gases or chemical products in order to increase the porosity of the resulting product.

The characteristics of the starting material, the conditions of the carbonisation process, and the catalysis process deeply affect the resulting charcoal [1]. The cherry bone is an agro-industrial residue produced in large quantities in the Jerte Valley Cooperative Association when manufacturing cherry or kirsch liquor. The advantage of its utilisation is a very suitable solution to obtain charcoal and activated carbon due to the current high demand.

In this work the methods of preparation of charcoal from the cherry bone (*H*) are described using different atmospheres. The temperature and time used in carbonisation are suitable for the subsequent production of activated carbon [2]. In Sec. 2 the characterization techniques are described. The results are presented and discussed in Sec. 3, and the conclusions obtained

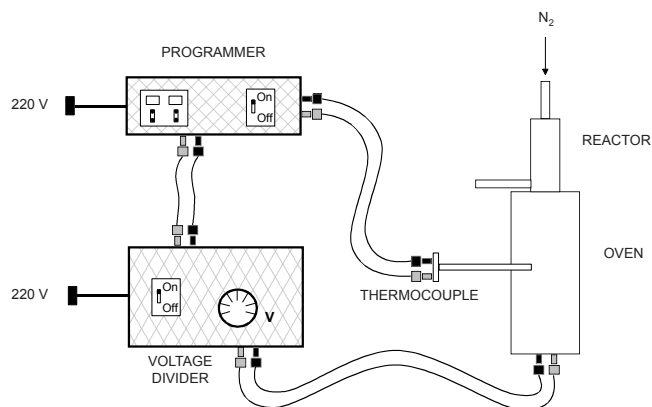


Figure 1: Experimental system used in the preparation of samples.

are highlighted in Sec. 4. Additionally, an appendix (Sec. 5) contains the experimental results in tabular form.

## 2. Experimental procedure

### 2.1. Charcoal preparation

The system used in the preparation of carbonates is shown schematically in Fig. 1. Basically, it consists of a vertical cylindrical furnace connected to a temperature/time programmer; and of a cylindrical stainless steel reactor, equipped with a threaded cap and two conduits for gas inlet and outlet. To study the influence of the heat treatment atmosphere, three samples have been prepared under the following conditions:

- Mass of *H*: 100g.

- Carbonisation atmosphere: atmosphere formed during heating, with and without nitrogen ( $200 \text{ cm}^3 \text{ min}^{-1}$ ) or air flow ( $200 \text{ cm}^3 \text{ min}^{-1}$ ).

\*Corresponding author

\*\*Principal investigator

Email addresses: araceli.venegas-gomez@strath.ac.uk (A. Venegas-Gomez), mgcorzo888@gmail.com (M. Gomez Corzo)

Table 1: Charcoal preparation

Sample	Precursor	Heating speed ( $^{\circ}\text{C min}^{-1}$ )	Flow of gas ( $\text{cm}^3 \text{min}^{-1}$ )	Isothermal temperature ( $^{\circ}\text{C}$ )	Isothermal time ( $h$ )
6002N	H	10	0	600	2
6002N	H	10	200 ( $N_2$ )	600	2
A6002N	H	10	200 (A)	600	2

- Initial heating temperature: room temperature.
- Heating rate:  $10^{\circ}\text{C min}^{-1}$ .
- Final heating temperature:  $600^{\circ}\text{C}$ .
- Isothermal heating time (t) at  $600^{\circ}\text{C}$ : 2 h.
- Atmosphere during cooling to room temperature: nitrogen ( $200 \text{ cm}^3 \text{ min}^{-1}$ ).

The samples are represented 6002N, N6002 and A6002N, respectively; 600 is the isothermal heating temperature; 2 indicates the number of hours of isothermal heating at  $600^{\circ}\text{C}$ ; N stands for nitrogen, indicating the atmosphere of heating and cooling if it is at the beginning, and the atmosphere of cooling if it is at the end; and A means air. This rate of heating is frequent in investigations of carbonisation processes. Brunner and Roberts [3] have already found that the carbonisation yield of the cellulose increases with the decrease in the heating rate. Mackay and Roberts [4] also found the same effect when studying the influence of pyrolysis conditions on the yield and microporosity of lignocellulosic carbonates. On the other hand, Kumar et al. [5] have shown that a carbonisation of acacia wood at  $1050^{\circ}\text{C}$  under rapid carbonisation clearly shows the absence of secondary carbon deposit, whereas the reverse occurs when carbonisation is slow. More recently, Lua and Guo [6] have found that  $10^{\circ}\text{C min}^{-1}$  and  $150 \text{ cm}^3 \text{ min}^{-1}$  are optimum conditions in the pyrolysis of carbonates prepared from residues of extracted palm fibre.

## 2.2. Charcoal characterisation

The charcoal and activated charcoal resulting from the following processes of preparation have been chemically and structurally characterized.

### 2.2.1. Chemical characterisation

The immediate chemical composition and the organic chemical structure have been determined [7].

### 2.2.2. Pore structure characterization

Samples have been characterized by applying density (packing, apparent and real), mercury porosimetry and scanning electron microscopy techniques [8]. In addition, they have been characterized by physisorption ( $\text{CO}_2$ , 273.15K;  $N_2$ , 77K) in a Micromeritics automatic apparatus (model ASAP 2010).

The method followed in the determination of adsorption isotherms is recorded in the literature [9]. Approximately 0.5g were degassed at  $250^{\circ}\text{C}$  for 24h under a dynamic vacuum of  $10^{-4}$  mm Hg ( $1 \text{ mmHg} = 1.3333 \cdot 10^2 \text{ Pa}$ ). After cooling, the samples adsorbed carbon dioxide to 273.15K or nitrogen at 77K, under different pressures.

The application of the DR [10], DA [11], and S [11] equations to the adsorption data has provided the micropore volumes of samples accessible to carbon dioxide,  $W_{DR}(\text{CO}_2)$ ,  $W_{DA}(\text{CO}_2)$  and  $W_S(\text{CO}_2)$ , and the values of the volume of micropores accessible to nitrogen,  $W_{DR}(N_2)$ . The values of the gas volume conversion factor in liquid volumes at the adsorption temperatures were  $1.831 \cdot 10^{-3}$  (density  $1.08 \text{ g cm}^{-3}$ ) [12] for carbon dioxide and  $1.547 \cdot 10^{-3}$  (density  $0.808 \text{ g cm}^{-3}$ ) [13] for nitrogen. The values taken for the affinity coefficient were 0.48 for carbon dioxide [14] and 0.34 for nitrogen [11].

The application of the DR equation has also provided the values for the parameter  $E_o$ , with which the mean values for the size of slit-shaped micropores ( $L_o$ ) have been calculated, by applying the semi-empirical correlation of Stoeckli and Ballerini [15].

The microporosity distributions have been calculated by the function proposed by Stoeckli [11] applied to the adsorption results of carbon dioxide at 273.15K.

From the nitrogen adsorption data, the samples specific surface area  $S_{BET}$  [9] was determined following the IUPAC recommendations: linearity range ( $p/p^o < 0.30$ ) and mean area of the  $N_2$  molecule occupied in the monolayer  $0.162 \text{ nm}^2$  [16]. From the carbon dioxide adsorption data, the specific micropore surface area of the samples  $S_{mi}$  has been determined [11]. The total surface area of the samples,  $S(\text{CO}_2)$  [17], with the values of  $W_{DR}(\text{CO}_2)$  and  $W_{DA}(\text{CO}_2)$ , and considering the mean area of the  $\text{CO}_2$  molecule as  $0.187 \text{ nm}^2$  [18].

## 3. Results and discussion

Of the three samples prepared in different atmospheres (6002N, N6002 and A6002N), the third is an activated carbon. In the following sections, to better understand the effects of the atmosphere during the heat treatment of H on the yield, the chemical composition and structure, as well as the pore structure of the samples, have been included.

### 3.1. Performance

As can be seen in Table 2, the yield is somewhat higher for 6002N compared to N6002 and significantly lower for A6002N. Considering that the volatile matter produced in the heat treatment of H passes through the pores of the carbonaceous material that is formed to its surface, the application of a nitrogen stream, in addition to providing an inert atmosphere for the pyrolysis, help to eliminate the volatile matter, forming a smaller amount of secondary carbon in the walls of the pores of N6002. When applying an air stream, the oxygen in it acts as a reagent, whereby the deposit of volatile matter in the pores of A6002N is significantly smaller.

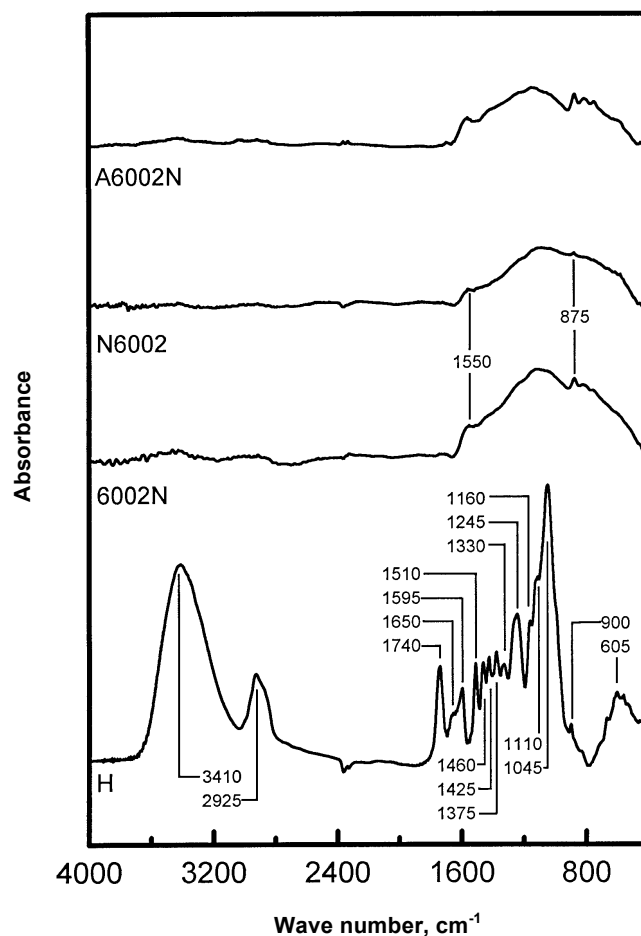
Table 2: Performance and immediate analysis of raw material and samples 6002N, N6002 and A6002N.

Sample	Performance (%)	Original sample reference (%)				Dry sample reference (%)			
		Humidity	Volatile matter	Ashes	Fixed Carbon	Volatile matter	Ashes	Fixed Carbon	
H	-	5.41	71.72	0.24	22.63	75.82	0.25	23.93	
6002N	26.32	6.94	7.75	1.36	83.95	8.33	1.46	90.21	
N6002	25.36	6.87	6.42	1.49	85.22	6.89	1.60	91.51	
A6002N	21.43	7.12	5.94	1.31	85.63	6.40	1.41	92.19	

### 3.2. Chemical composition and structure

According to the previous comments, the immediate analyses (Table 2) show that decreasing the yield also decreases the volatile matter. The low ash content and high fixed carbon content of the three samples are favourable properties to be used as activated carbon precursors.

According to the *FTIR* spectra (Fig. 2), the thermal treatments of *H* have produced strong changes in the chemical-organic structure of the material. In the spectra of 6002N, N6002 and A6002N, a wide band at wavelengths less than  $1600\text{ cm}^{-1}$  can be observed, which is the result of the overlap of several individual absorption bands. The resulting samples contain aromatic rings (at  $1550\text{ cm}^{-1}$ ), with the highest amount of aromatic *C – H* bonds for 6002N and A6002N (bands better defined at  $900\text{--}700\text{ cm}^{-1}$ ). Oxygen forms *C – O* bonds ( $1300\text{--}1000\text{ cm}^{-1}$  band), without the air atmosphere leading to a more oxygenated structure in the case of A6002N; at  $1240\text{ cm}^{-1}$  could correspond to asymmetric deformation vibrations in *C – O – C* bonds in a single layer, and the band at  $1110\text{ cm}^{-1}$  to *C – O – C* bonds between graphite layers.

Figure 2: *FTIR* spectra of *H*, 6002N, N6002 and A6002N.

### 3.3. Pores structure

The values of the density and the total volume of pores accessible to helium at room temperature are given in Table 3. In contrast to *H*, the density values (packing density  $\rho$ , mercury accessible density  $\rho_{Hg}$ , and helium accessible density  $\rho_{He}$ ) indicate that the three heat treatments have developed porosity. The  $V_{He}$  values show that at least the pore volume has doubled. The highest pore volume of A6002N is due to the reactive oxygen atmosphere.

Table 3: Raw material and samples 6002N, N6002 and A6002N: densities and total pore volume.

Muestra	$\rho$ ( $g\ cm^{-3}$ )	$\rho_{Hg}$ ( $g\ cm^{-3}$ )	$\rho_{He}$ ( $g\ cm^{-3}$ )	$V_{He}$ ( $cm^{-3}\ g^{-1}$ )
H	0.76	1.09	1.38	0.193
6002N	0.62	1.02	1.76	0.412
N6002	0.59	1.00	1.71	0.415
A6002N	0.59	0.91	1.72	0.518

Table A.8 to Table A.13 of the appendix give the data on the adsorption of carbon dioxide at 273.15K and nitrogen at 77K. With them, the isotherms of Fig. 3 and Fig. 4 have been obtained, showing that the treatment atmosphere has a greater influence on nitrogen adsorbent capacity than on the adsorption capacity of carbon dioxide.

According to the classification of the isotherms of physisorption of the IUPAC [17], the isotherms of Fig. 4 can be considered of type I, characteristics of microporous solids. More precisely, the type  $I_b$  [19] isotherm can be considered, especially the 6002N. As nitrogen adsorption grows relatively little when  $p/p^o$  increases, the samples have a small amount of mesopores. Therefore, the positions and shapes of the nitrogen adsorption isotherms indicate that the development of the broad microporosity of the samples follows the sequence  $A6002N > N6002 \gg 6002N$ , and that the development of mesoporosity is somewhat greater in A6002N and N6002.

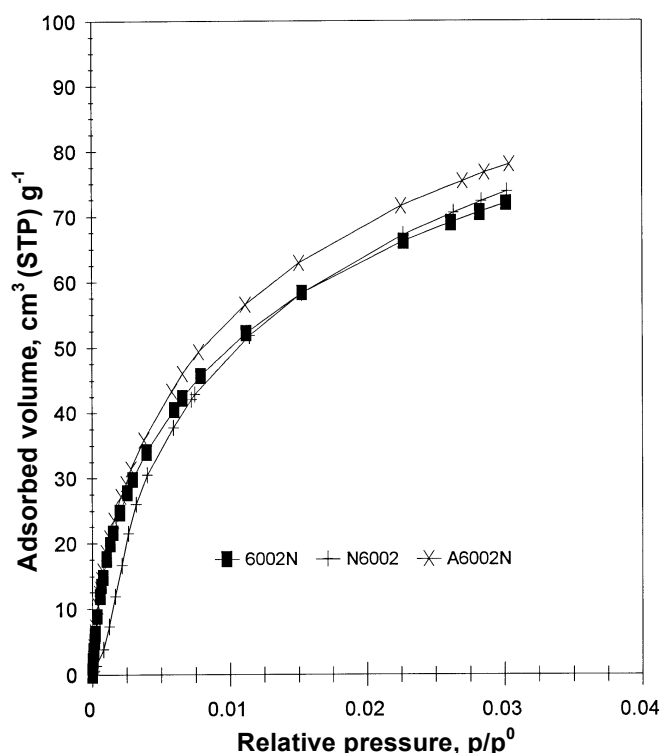


Figure 3: Carbon dioxide adsorption isotherms at 273.15K of 6002N, N6002 and A6002N.

The calculations made by applying the equations DR, DA and S to the isotherms of Fig. 3 and Fig. 4 are also given in

Table A.8 to Table A.13. The adjustments of these equations are shown in Fig. 5 to Fig. 8. The DR ( $CO_2$ ) setting of 6002N (Fig. 5) is of type A of those indicated by Marsh [17], while the DR ( $N_2$ ) setting (Fig. 8) can be considered as type D [17]. Therefore, according to the results found by Rodriguez-Reinoso et al. [20] in characterizing almond shell charcoal, the nitrogen adsorption at 77K is kinetically restricted at 6002N, while adsorption of carbon dioxide at 273.15K is not. The rest of the adjustments can be considered of type A [17].

The values for the parameters in equations DR, DA and S (Table 4 and Table 5) allow to establish that  $W_S(CO_2) < W_{DR}(CO_2)$  and that  $W_S(CO_2) < W_{DA}(CO_2)$  for each sample. Therefore, the volume of narrow micropores of each carbon depends on the applied equation. As  $W_{DR}(CO_2) > W_{DR}(N_2)$ , the microporous structure of the three samples consists mainly of narrow micropores. A6002N is the sample with the largest volume of narrow and wide micropores.

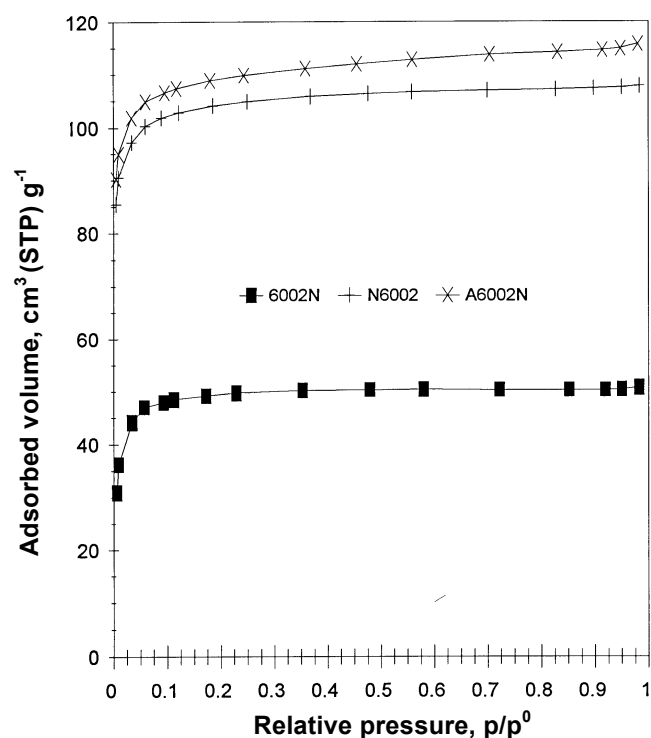


Figure 4: Nitrogen adsorption isotherms at 77K of 6002N, N6002 and A6002N.

Table 5: Parameters of the S equation applied to the adsorption isotherms of carbon dioxide at 273.15 K of samples 6002N, N6002 and A6002N.

Sample	$K_0$ ( $nm\ kJ\ mol^{-1}$ )	$W_S(CO_2)$ ( $cm^3\ g^{-1}$ )	$\nu$	$a$ ( $nm^{-1}$ )
6002N	22.08	0.158	5.35	9.22
N6002	20.19	0.158	7.47	18.73
A6002N	24.41	0.177	4.27	5.02

All the values of the characteristic energy of the DR equation (Table 4) are included in the range of characteristic energies 30-35 to 17-18  $kJ\ mol^{-1}$  [11], resulting in  $E_0(CO_2) > E_0(N_2)$ .

Table 4: Parameters of the *DR* and *DA* equations applied to the adsorption isotherms of samples 6002N, N6002 and A6002N.

Sample	DR Equation				DA Equation		
	$W_{DR}(CO_2)$ ( $cm^3 g^{-1}$ )	$E_0(CO_2)$ ( $kJ mol^{-1}$ )	$W_{DR}(N_2)$ ( $cm^3 g^{-1}$ )	$E_0(N_2)$ ( $kJ mol^{-1}$ )	$W_{DA}(CO_2)$ ( $cm^3 g^{-1}$ )	$E_0(CO_2)$ ( $kJ mol^{-1}$ )	$n(CO_2)$
6002N	0.214	23.43	0.078	21.06	0.239	22.31	1.91
N6002	0.253	22.67	0.166	21.03	0.212	24.51	2.16
A6002N	0.211	24.14	0.175	20.86	0.305	20.45	1.73

The values of  $K_0$  (Table 5) are between 16 and 35  $nm kJ mol^{-1}$  [21].

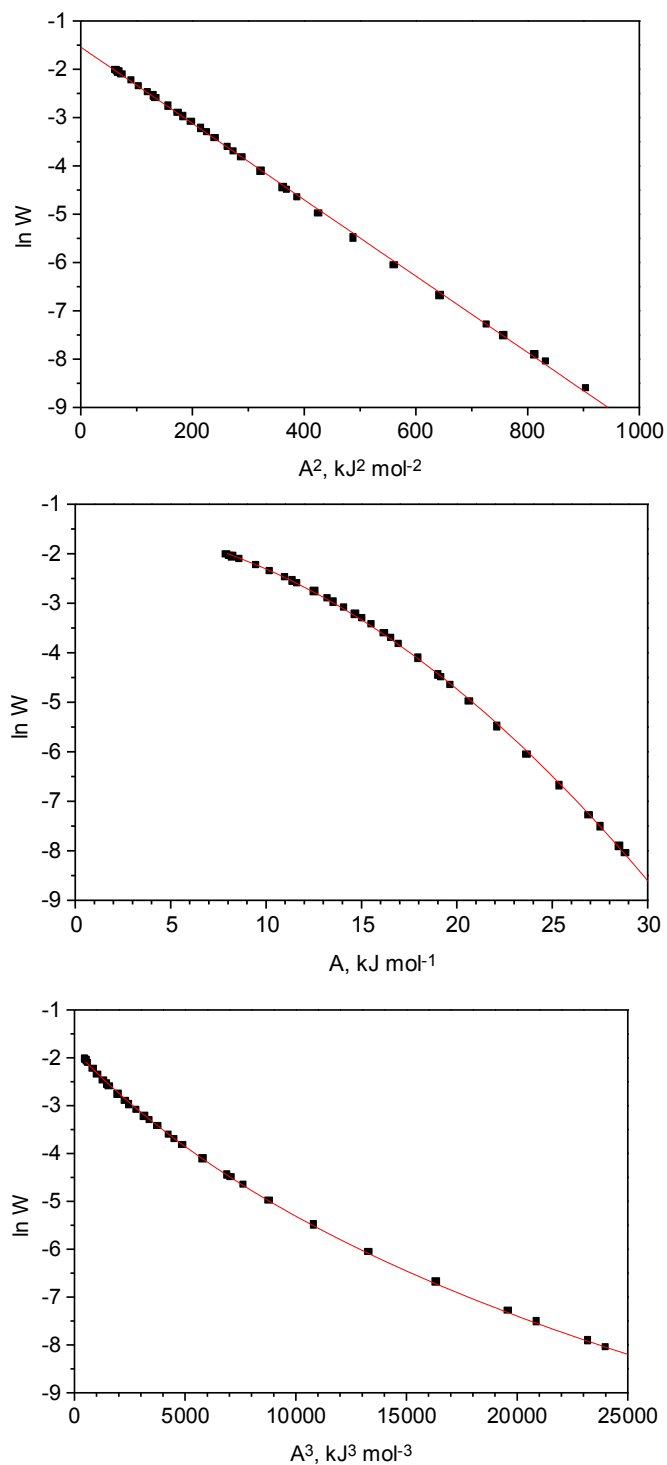


Figure 5: Sample 6002N: application of the *DR* (above), *DA* (medium) and *S* (below) equations to the adsorption isotherm of carbon dioxide at 273.15K.

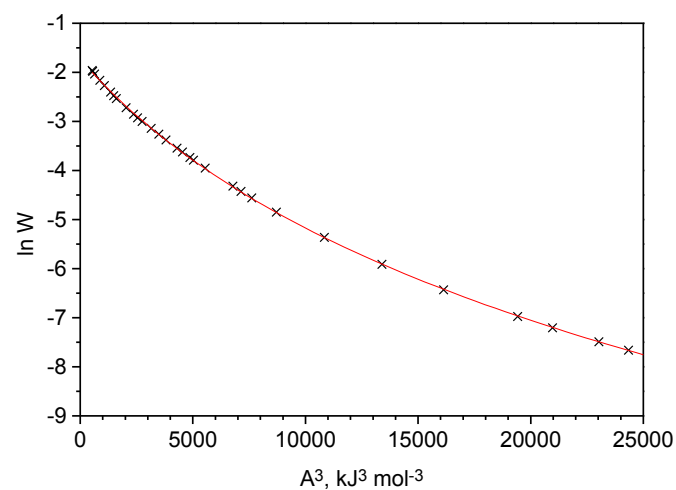
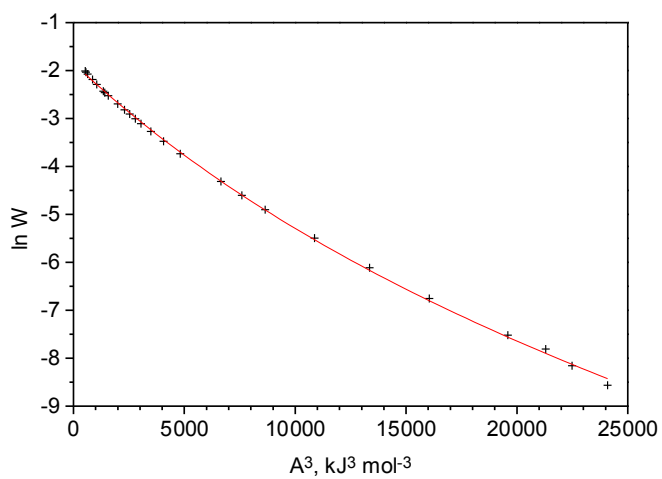
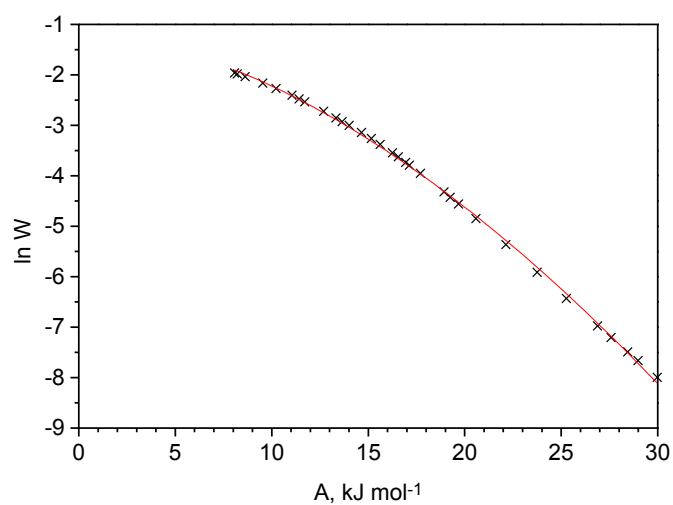
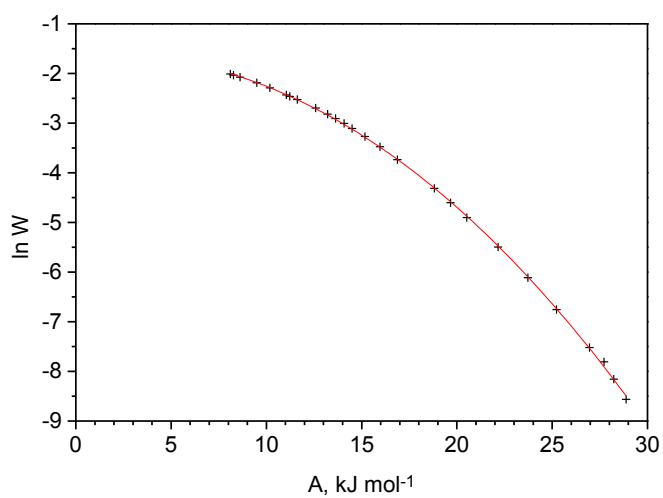
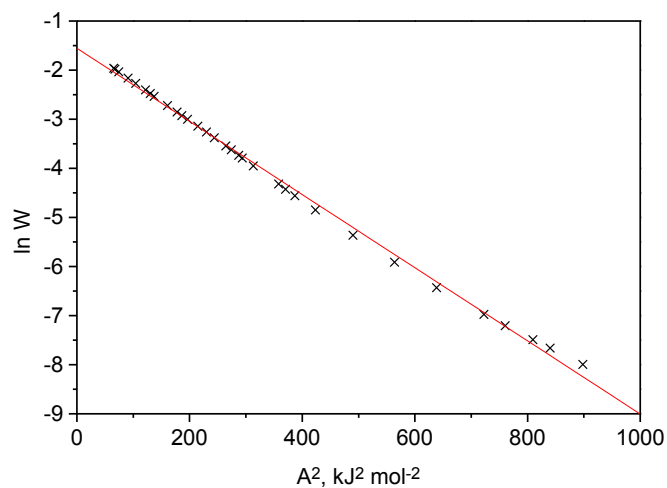
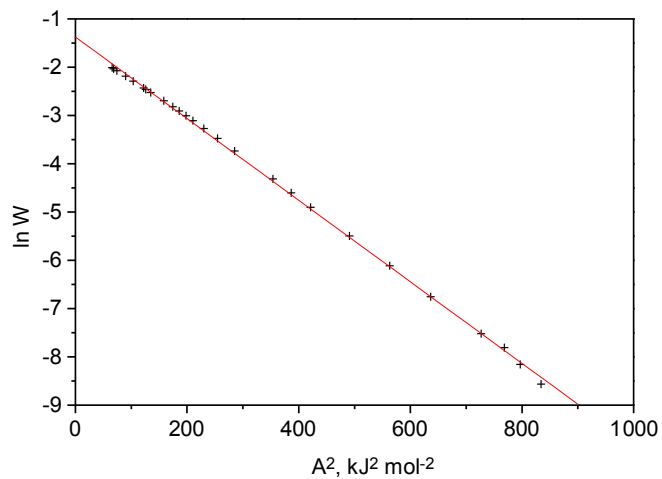


Figure 6: Sample N6002: application of the *DR* (above), *DA* (medium) and *S* (below) equations to the adsorption isotherm of carbon dioxide at 273.15K.

Figure 7: Sample A6002N: application of the *DR* (above), *DA* (medium) and *S* (below) equations to the adsorption isotherm of carbon dioxide at 273.15K.

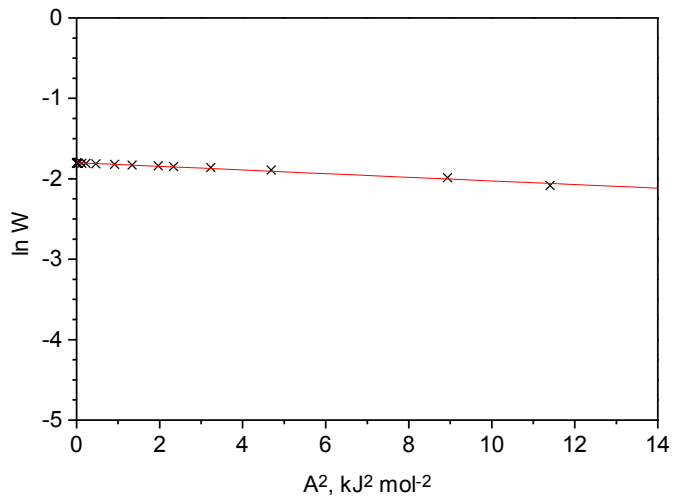
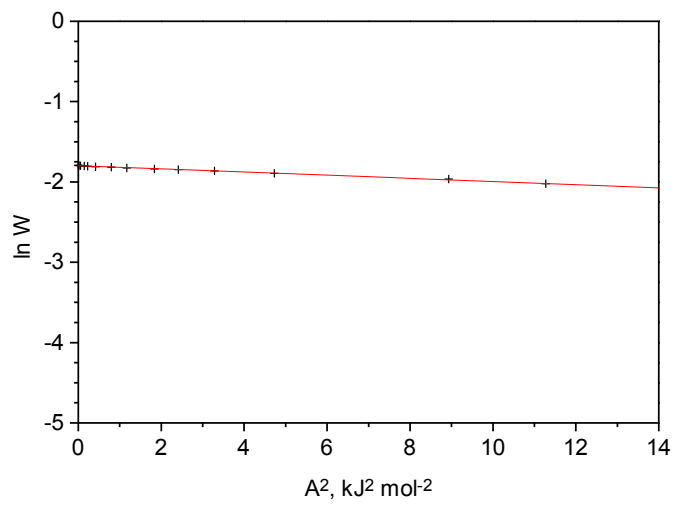
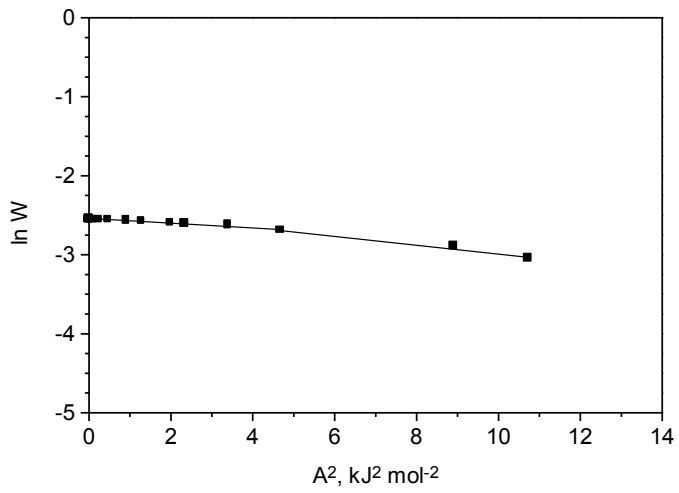


Figure 8: Samples 6002N (top), N6002 (medium) and A6002N (below): application of the *DR* equation to nitrogen adsorption isotherms at 77K.

The fact that the value of  $n(CO_2)$  for A6002N is the smallest of the three (Table 4) indicates that the narrow micropore structure of this sample is the most heterogeneous. This can be observed in the representations of Fig. 9, which have the same appearance, differing in the width of the curves and in the maximum value of  $dW/dL$ .

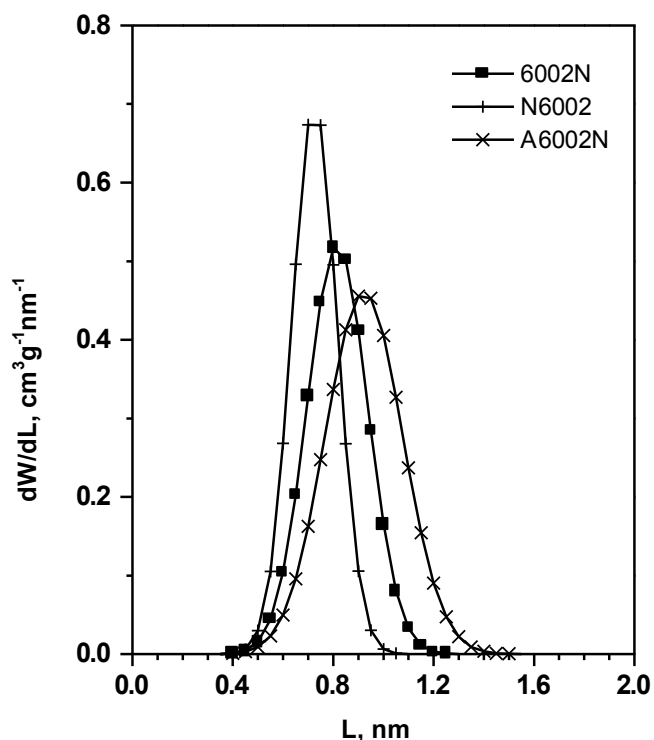


Figure 9: Distributions of micropore sizes determined by applying the Stoeckli method to the adsorption isotherms of carbon dioxide at 273.15K of samples 6002N, N6002 and A6002N.

With values of  $E_0(CO_2)$  and  $E_0(N_2)$ , the mean micropore widths  $L_0(CO_2)$  and  $L_0(N_2)$  have been calculated (Table 3.5), which are included in the range 0.4-2 nm [21].

Further information on the microporous structure of the samples is derived from the values of the surface area (Table 6). The calculations made when applying the  $BET(N_2)$  equation are given in Table A.11 to Table A.13 and the  $BET(N_2)$  settings are shown in Fig. 10; with the highest value of  $S_{BET}(N_2)$  corresponding to A6002N. From the Stoeckli-Ballerini relation [21], the values of the area of the walls of micropores such as  $S_{mi}(CO_2) > S_{mi}(N_2)$  have been obtained for each sample.  $S_{BET}(N_2) > S_{mi}(N_2)$  for each sample because  $S_{BET}(N_2)$  represents the equivalent area of the monolayer, which would coincide with  $S_{mi}(N_2)$  if the micropores accommodated two adsorbate layers. For the same reason,  $S_{DR}(CO_2) > S_{mi}(CO_2)$  and  $S_{DA}(CO_2) > S_{mi}(CO_2)$ . The results obtained in the characterization of the microporous structure of 6002N and N6002, can be interpreted considering that a greater quantity of alquitrona matter, deposited and decomposed in the microporous network of 6002N, partially fills or blocks more micropores than in N6002, forming more constrictions. Although both samples are

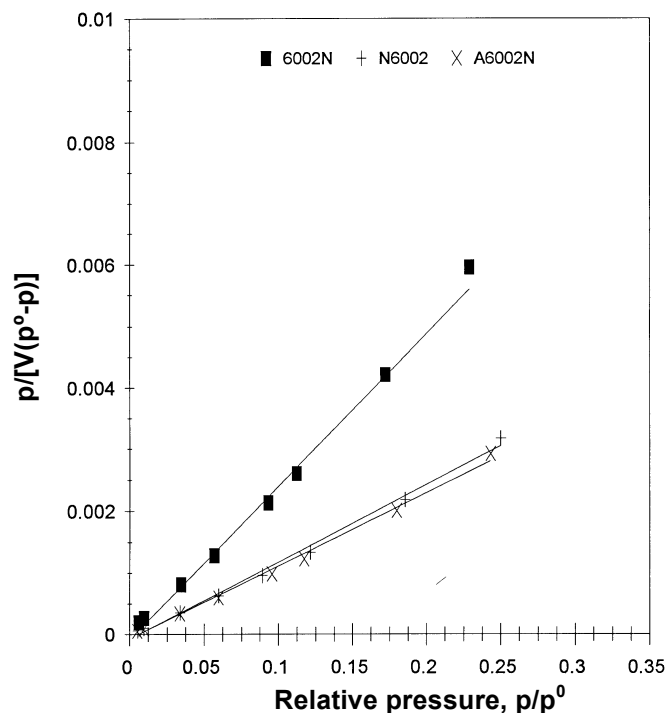


Figure 10:  $BET$  settings ( $N_2$ , 77K) of samples 6002N, N6002 and A6002N.

mainly formed by narrow micropores, they have more uniform widths in N6002. In A6002N, in addition to the drag of volatile matter produced in the heat treatment of  $H$ , oxygen reaction of the air stream applied with that matter must occur, preventing its deposit in the carbonaceous material being formed. In comparison with the other two samples, a microporous structure formed mainly of narrow micropores is obtained as well, but in this case is more heterogeneous, more open, and with a larger volume of micropores.

Regarding the non-microporous structure of the samples, it has been commented previously that the isotherms of Fig. 4 indicate that each of them has a small amount of mesopores, since nitrogen adsorption at 77K grows relatively little when  $p/p^0$  increases. As can be seen in Table 7, the mesopore volume values ( $V_{me}$ ), determined by mercury porosimetry, are the same ( $0.006 \text{ cm}^3 \text{ g}^{-1}$ ) for all three samples. In contrast, the macropore volume values ( $V_{ma}$ ) are almost the same for 6002N and N6002, and higher in the case of A6002N. Consequently, the values of  $V_{ma}$  and the cumulative volume of mesopores and macropores ( $V_{Hg}$ ) are almost the same, i.e. it turns out that the non-microporous structure of the samples consists mainly of macropores. From the same table, it is also deduced that the three samples have a high volume of macropores compared to  $H$ .

Table 6: Average size of micropores and specific surface areas of samples 6002N, N6002 and A6002N.

Sample	$S_{BET}(N_2)$ ( $m^2 g^{-1}$ )	$L_O(CO_2)$ (nm)	$S_{mi}(CO_2)$ ( $m^2 g^{-1}$ )	$L_O(CO_2)$ (nm)	$S_{mi}(N_2)$ ( $m^2 g^{-1}$ )	$S_{DR}(CO_2)$ ( $m^2 g^{-1}$ )	$S_{DA}(CO_2)$ ( $m^2 g^{-1}$ )
6002N	171	0.90	476	1.12	139	589	558
N6002	321	0.96	527	1.12	296	696	583
A6002N	369	0.85	496	1.14	307	581	839

Table 7: Macropores and mesopores volumes for the samples 6002N, N6002 and A6002N

Muestra	$V_{ma}$ ( $cm^3 g^{-1}$ )	$V_{me}$ ( $cm^3 g^{-1}$ )	$V_{Hg}$ ( $cm^3 g^{-1}$ )
H	0.122	0.000	0.122
6002N	0.246	0.006	0.252
N6002	0.248	0.006	0.254
A6002N	0.291	0.006	0.297

The representations of Fig. 11 have been obtained with the recorded mercury porosimetry data given in Table A.14 to Table A.16. The variations of  $V_{Hg}$  with the pore radius are practically the same for 6002N and N6002, which shows that the non-microporous structure is not modified by the application of the nitrogen flow during the heat treatment of *H*. In contrast,  $V_{Hg}$  for A6002N is greater for pore radii smaller than 400 nm, demonstrating that the air atmosphere produces a greater macroporous development. The representation of the derivative of  $V_{Hg}$  versus the pore radius is essentially unimodal, with a peak centred at approximately 200 nm for both the raw material and the three samples prepared.

The results obtained in the characterization of the pore structure make it possible to specify that the effect of the reactive action of oxygen in the air atmosphere mainly results in a better development of the broad microporosity and the macroporosity.

#### 4. Conclusions

In view of the results presented and discussed in this paper, the following conclusions can be drawn:

1. Residual cherry bone treatments of kirsch production carried out at the final heating temperature of 600°C, with or without the application of an equal flow of nitrogen or air, are three processes of different performance in material carbonaceous. The yield is somewhat lower by applying the nitrogen stream and about 5% lower by applying the air stream.

2. The three prepared samples differ in the immediate chemical composition, having a low ash content, around 1.5%. The oxygen forms ether-like structure, without the air atmosphere leading to a more oxygenated structure.

3. Compared with the raw material, the volume of pores accessible to helium at room temperature is at least doubled. The application of the air stream produces a more significant porous development.

4. The microporous structures of the samples are mainly formed by narrow micropores, with greater heterogeneity of sizes when air is applied. However, the differences are more

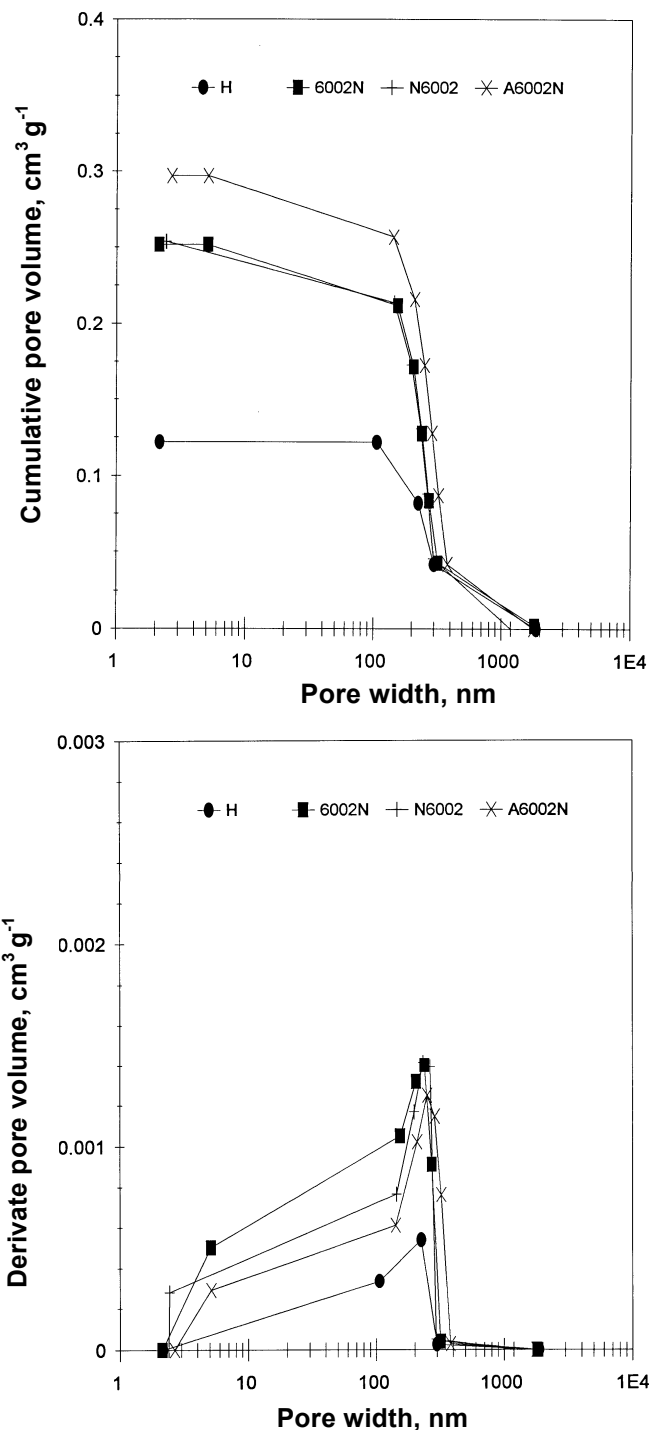


Figure 11: Distributions of pore sizes in the mesopore and macropore intervals of samples 6002N, N6002 and A6002N determined by mercury porosimetry.

significant in wide microporosity; the volume of wide micropores or the *BET* surface area ( $N_2$ , 77K) doubles when nitrogen is applied; and with air improves the development of this microporosity. These results can be interpreted by considering that a greater quantity of tarry matter, deposited and decomposed in the microporous network of the carbonisation prepared without application of nitrogen or air current, partially fills or blocks more micropores, forming more constrictions.

5. Regarding the non-microporous structure, the development is important compared to the raw material. The application of the nitrogen stream does not improve the development of the structure of macropores and mesopores, while the air current develops macroporosity. On the other hand, none of them has any influence on the development of mesoporosity.

## 5. Acknowledgements

The authors appreciate support by the Department of Inorganic Chemistry, Faculty of Science, University of Extremadura.

## References

- [1] Shafizadesh, F., Overend, R., Milne, T., Mudge, L.. Fundamentals of Thermochemical Biomass Conversion. Elsevier Applied Science Publishers, London; 1985.
- [2] Valenzuela Calahorra, C.. Introduccin a la Química Inorgánica. Editorial McGraw-Hill Interamericana de Espaa, Madrid; 1999.
- [3] Brunner, P., Roberts, P.. The significance of heating rate on char yield and char properties in the pyrolysis of cellulose. Carbon 1982;18:217.
- [4] Mackay, D., Roberts, P.. The influence of pyrolysis conditions on yield and microporosity of lignocellulosic chars. Carbon 1982;20:95.
- [5] Kumar, M., Gupta, T.. Effects of carbonisation conditions on the yield and chemical composition of acacia and eucalyptus wood chars. Biomass and Bioenergy 1992;3:411.
- [6] Lua, A., Guo, J.. Preparation and characterization of chars from oil palm waste. Carbon 1998;36:1663.
- [7] Pastor-Villegas, J., Gámez-Serrano, V., Durán-Valle, C., Higes-Rolando, F.. Chemical study of extracted rockrose and of chars and activated carbons prepared at different temperatures. J Anal Appl Pyrolysis 1999;50:53–61.
- [8] Pastor-Villegas, J., Durán-Valle, C.. Pore structure of chars and activated carbons prepared using carbon dioxide at different temperatures from extracted rockrose. J Anal Appl Pyrolysis 2001;57:1–13.
- [9] Rouquerol, J., Avnir, D., Fairbridge, C., Everett, D., Haynes, J., Pernicone, N., et al. Recommendations for the characterization of porous solids. Pure Appl Chem 1994;66:1739–1758.
- [10] Dubinin, M.. Fundamentals of the theory of adsorption in micropores of carbon adsorbents: Characteristics of their adsorption properties and microporous structures. Carbon 2001;27:457.
- [11] Stoeckli, H., Patrick, J.. Porosity in Carbons. Characterization and Applications, chapter 3. Edward Arnold, London; 1995.
- [12] Toda, Y., Hatami, M., Toyoda, S., Yoshida, Y., Honda, H.. Recommendations for the characterization of porous solids. Fuel 1971;50:187–200.
- [13] Marsh, H., Rand, B.. The characterization of microporous carbons by means of the dubinin-radushkevich equation. J Colloid Interface Sci 1970;33:101–116.
- [14] Parra, J., Pis, J., Sousa, J., Pajares, J., Bansal, R.. Effect of coal preoxidation on the development of microporosity in activated carbons. Carbon 1996;34:783–787.
- [15] Stoeckli, F., Ballerini, L.. Evolution of microporosity during activation of carbon. Fuel 1991;70:557559.
- [16] Sing, K., Everett, D., Hault, R., Moscou, L., Pierotti, R., Rouquerol, J., et al. Reporting physisorption data for gas/solid systems with special reference to the determination of surface area and porosity. Pure Appl Chem 1985;57:603–619.
- [17] Byrne, J., Marsh, H., Patrick, J.. Porosity in Carbons. Characterization and Applications, chapter 1. Edward Arnold, London; 1995.
- [18] Rodríguez-Reinoso, F., Linares-Solano, A.. Microporous structure of activated carbons as revealed by adsorption methods. PA Thrower (Ed), Chemistry and Physics of Carbon 1989;21:1–146.
- [19] Rouquerol, F., J., R., Sing, K.. Adsorption by Powders and Porous Solids, chapter 13. Academic Press, San Diego; 1995.
- [20] Rodríguez-Reinoso, F., López-González, J., Berenguer, C.. Activated carbons from almond shells: Preparation and characterization by nitrogen adsorption. Carbon 1982;20:513–518.
- [21] Stoeckli, H.. Microporous carbons and their characterization: The present state of the art. Carbon 1990;28:1–6.

## Appendix A.

Table A.8: Sample 6002N: adsorption data of carbon dioxide at 273.15K and values calculated by applying the equations  $DR$ ,  $DA$  and  $S$ .

$P$ ( $mm\ Hg$ )	$\rho/\rho^o$	$V$ ( $cm^3$ CNPT $g^{-1}$ )	$A$ ( $kJ\ mol^{-1}$ )	$A^2$ ( $kJ^2\ mol^{-2}$ )	$A^3$ ( $kJ^3\ mol^{-3}$ )	$\ln W$
0.0444	0.000002	0.0996	30.0792	904.7586	27214.4204	-8.6095
0.0784	0.000003	0.1744	28.8556	832.6450	24026.4628	-8.0493
0.0915	0.000004	0.1991	28.5270	813.7908	23215.0265	-7.9168
0.1412	0.000005	0.2969	275.364	7.582.557	208.796.662	-7.5173
0.1804	0.000007	0.3719	26.9568	726.6688	19588.6624	-7.2920
0.3660	0.000014	0.6767	253.804	6.441.651	163.491.737	-6.6934
0.7660	0.000029	1.2670	23.6999	561.6873	13311.9570	-6.0662
1.5398	0.000059	2.2541	22.1153	489.0878	10816.3388	-5.4901
2.9253	0.000112	3.7269	20.6594	426.8116	8817.6793	-4.9873
4.4886	0.000172	5.1766	19.6884	387.6312	7631.8198	-4.6587
5.5735	0.000213	6.0522	19.1964	368.4999	7073.8525	-4.5025
5.9368	0.000227	6.3825	19.0535	363.0353	6917.0870	-4.4493
9.5052	0.000364	8.8541	17.9847	323.4500	5817.1569	-4.1220
14.7650	0.000565	11.9042	16.9846	288.4780	4899.6940	-3.8260
17.8315	0.000682	13.5062	16.5561	274.1035	4538.0772	-3.6997
20.6757	0.000791	14.8169	16.2200	263.0877	4267.2761	-3.6071
27.8621	0.001066	17.7045	15.5424	241.5657	3754.5057	-3.4291
34.3793	0.001315	19.9140	15.0652	226.9592	3419.1772	-3.3115
40.1201	0.001535	21.5938	14.7145	216.5169	3185.9403	-3.2305
52.7912	0.002019	24.8083	14.0913	198.5636	2798.0103	-3.0917
66.7013	0.002552	27.7788	13.5601	183.8759	2493.3719	-2.9786
77.5607	0.002967	29.8390	13.2175	174.7029	2309.1395	-2.9071
103.8334	0.003972	34.0733	12.5551	157.6297	1979.0514	-2.7744
155.8063	0.005960	40.5312	11.6334	135.3370	1574.4350	-2.6008
171.3216	0.006554	42.3890	11.4179	130.3678	1488.5235	-2.5560
206.2290	0.007889	45.7439	10.9967	120.9281	1329.8145	-2.4798
292.3852	0.011185	52.2290	10.2040	104.1209	1062.4464	-2.3473
398.8145	0.015256	58.3191	9.4990	90.2311	857.1055	-2.2370
592.4875	0.022664	66.2432	8.6001	73.9614	636.0746	-2.1096
683.1950	0.026134	69.0761	8.2766	68.5018	566.9607	-2.0677
737.8580	0.028225	70.6440	8.1018	65.6389	531.7922	-2.0452
787.8205	0.030136	71.9675	7.9530	63.2501	503.0279	-2.0267

Table A.9: Sample N6002: carbon dioxide adsorption data at 273.15K and calculated values when applying the equations  $DR$ ,  $DA$  and  $S$ .

$P$ ( $mm\ Hg$ )	$\rho/\rho^o$	$V$ ( $cm^3$ $CNPTg^{-1}$ )	$A$ ( $kJ\ mol^{-1}$ )	$A^2$ ( $kJ^2\ mol^{-2}$ )	$A^3$ ( $kJ^3\ mol^{-3}$ )	$\ln W$
0.0665	0.000003	0.1044	28.8797	834.0362	24086.7018	-8.5624
0.0990	0.000004	0.1568	28.2264	796.7278	22488.7321	-8.1557
0.1385	0.000005	0.2218	27.7196	768.3771	21299.1168	-7.8089
0.1846	0.000007	0.2956	26.9555	726.5988	19585.8327	-7.5216
0.3862	0.000015	0.6358	25.2247	636.2855	16050.1117	-6.7558
0.7619	0.000029	1.2115	23.7276	562.9978	13358.5713	-6.1110
1.5214	0.000058	2.2415	22.1535	490.7757	10872.3791	-5.4957
3.1174	0.000119	4.0672	20.5214	421.1261	8642.0788	-4.8999
4.5393	0.000174	5.4694	19.6585	386.4583	7597.2079	-4.6037
6.6079	0.000253	7.3199	18.8084	353.7575	6653.6273	-4.3123
15.4461	0.000591	13.0613	16.8817	284.9915	4811.1387	-3.7332
23.2085	0.000888	16.8906	15.9571	254.6276	4063.1054	-3.4761
32.8792	0.001258	20.7658	15.1661	230.0094	3488.3357	-3.2696
44.0910	0.001687	24.4613	14.4997	210.2411	3048.4308	-3.1058
53.1411	0.002033	27.0452	14.0760	198.1343	2788.9420	-3.0054
64.5288	0.002468	29.8613	13.6357	185.9320	2535.3104	-2.9063
77.9023	0.002980	32.6578	13.2076	174.4400	2303.9301	-2.8168
102.5393	0.003922	36.8552	12.5838	158.3517	1992.6650	-2.6959
156.9435	0.006003	43.6577	11.6171	134.9578	1567.8228	-2.5265
186.8347	0.007147	46.6836	11.2210	125.9109	1412.8459	-2.4595
201.6770	0.007715	48.1071	11.0473	122.0435	1348.2553	-2.4295
295.8500	0.011317	55.3769	10.1772	103.5761	1054.1179	-2.2887
400.4177	0.015317	61.2780	9.4899	90.0584	854.6455	-2.1875
589.4877	0.022549	68.6743	8.6117	74.1607	638.6471	-2.0735
685.0053	0.026203	71.5645	8.2706	68.4028	565.7325	-2.0323
735.7792	0.028145	73.0275	8.1082	65.7435	533.0637	-2.0121
786.4701	0.030085	74.3473				

Table A.10: Sample A6002N: carbon dioxide adsorption data at 273.15K and calculated values when applying the equations  $DR$ ,  $DA$  and  $S$ .

$P$ (mm Hg)	$\rho/\rho^o$	$V$ ( $cm^3$ CNPT $g^{-1}$ )	$A$ ( $kJ\ mol^{-1}$ )	$A^2$ ( $kJ^2\ mol^{-2}$ )	$A^3$ ( $kJ^3\ mol^{-3}$ )	$\ln W$
0.0485	0.000002	0.1845	29.9702	898.2116	26919.5612	-7.9930
0.0750	0.000003	0.2570	28.9803	839.8572	24339.3031	-7.6616
0.0947	0.000004	0.3050	28.4512	809.4694	23030.3546	-7.4903
0.1392	0.000005	0.4055	27.5770	760.4925	20972.1222	-7.2055
0.1891	0.000007	0.5113	26.8815	722.6124	19424.8704	-6.9737
0.3850	0.000015	0.8815	25.2661	638.3760	16129.2758	-6.4290
0.7513	0.000029	14.820	237.481	563.9725	133.932.785	-59.095
1.5303	0.000059	2.5552	22.1325	489.8471	10841.5364	-5.3648
3.0363	0.000116	4.2809	20.5765	423.3918	8711.9146	-4.8487
45.148	0.000173	5.7302	19.6755	387.1267	7616.9242	-4.5571
5.4457	0.000208	6.5424	19.2498	370.5556	7133.1298	-4.4246
6.2731	0.000240	72.648	18.9286	358.2914	6781.9501	-4.3199
10.7723	0.000412	10.4980	17.7007	313.3134	5545.8536	-3.9517
13.8235	0.000529	12.3790	17.1343	293.5843	5030.3610	-3.7869
15.0134	0.000574	13.0436	16.9469	287.1957	4867.0629	-3.7346
17.8498	0.000683	14.5712	16.5535	274.0183	4535.9625	-3.6238
20.3385	0.000778	15.8149	16.2573	264.2984	4296.7660	-3.5419
26.8949	0.001029	18.6249	15.6226	244.0668	3812.9682	-3.3784
32.9572	0.001261	20.9222	15.1611	229.8600	3484.9386	-3.2621
41.1737	0.001575	23.5739	14.6556	214.7865	3147.8232	-3.1428
54.6211	0.002089	27.2275	14.0139	196.3883	2752.1575	-2.9987
64.1420	0.002454	29.2241	13.6490	186.2944	2542.7266	-2.9279
73.9113	0.002827	31.4580	13.3270	177.6099	2367.0128	-2.8542
98.1135	0.003753	35.9158	12.6838	160.8775	2040.5305	-2.7217
150.7139	0.005765	43.3502	11.7089	137.0992	1605.2857	-2.5336
171.7085	0.006568	46.0509	11.4127	130.2507	1486.5184	-2.4731
202.0149	0.007728	49.3700	11.0436	121.9618	1346.9011	-2.4036
290.4455	0.011110	56.5785	10.2191	104.4297	1067.1753	-2.2673
3.928.175	0.015026	62.9364	9.5334	90.8862	866.4571	-2.1608
587.7558	0.022483	71.5672	8.6183	74.2750	640.1239	-2.0323
704.8903	0.026964	75.4027	8.2056	67.3317	552.4967	-1.9800
746.8822	0.028570	76.6820	8.0742	65.1924	526.3748	-1.9632
793.4777	0.030353	77.9859				

Table A.11: Sample 6002N: nitrogen adsorption data adsorbed at 77K and calculated values when applying the equations *DR* and *BET*.

$P$ (mm Hg)	$\rho/\rho^o$	$V$ (cm <sup>3</sup> CNPTg <sup>-1</sup> )	$A^2$ (kJ <sup>2</sup> mol <sup>-2</sup> )	$\ln W$	$p/[V(\rho^o - \rho)]$
4.4216	0.006161	30.9885	10.7126	-3.0378	0.0002
6.9039	0.009675	36.2258	8.8966	-2.8817	0.00027
24.6732	0.034728	44.2173	4.6695	-2.6823	0.000814
40.4981	0.057031	47.0159	<b>3.3926</b>	<b>-2.621</b>	0.001286
66.2262	0.093246	47.9904	<b>2.3279</b>	<b>-2.6004</b>	0.002143
79.7496	0.112272	48.5271	<b>1.9777</b>	<b>-2.5893</b>	0.002606
122.3525	0.172296	49.2656	<b>1.2789</b>	<b>-2.5742</b>	0.004223
162.6178	0.228907	49.8194	<b>0.8991</b>	<b>-2.563</b>	0.005959
250.4609	0.352558	50.2161	<b>0.4495</b>	<b>-2.5551</b>	
340.3829	0.479136	50.3601	<b>0.2239</b>	<b>-2.5522</b>	
412.3754	0.580476	50.4156	<b>0.1223</b>	<b>-2.5511</b>	
512.9403	0.722035	50.3741	<b>0.0439</b>	<b>-2.552</b>	
605.2672	0.851998	50.3204	<b>0.0106</b>	<b>-2.553</b>	
653.2846	0.919589	50.3883	<b>0.0029</b>	<b>-2.5517</b>	
674.7671	0.949828	50.4776	<b>0.0011</b>	-2.5499	
698.0543	0.982609	50.7806	<b>0.0001</b>	<b>-2.5439</b>	

The values in bold are those used in the *DR* setting.

Table A.12: Sample N6002: nitrogen adsorption data adsorbed at 77K and calculated values when applying the equations *DR* and *BET*.

$P$ (mm Hg)	$\rho/\rho^o$	$V$ (cm <sup>3</sup> CNPTg <sup>-1</sup> )	$A^2$ (kJ <sup>2</sup> mol <sup>-2</sup> )	$\ln W$	$p/[V(\rho^o - \rho)]$
3.8786	0.005405	85.5065	11.2708	-2.0228	0.000064
6.8781	0.009584	90.579	8.9332	-1.9652	0.000107
24.425	0.034027	97.2627	4.7264	-1.894	0.000362
42.8562	0.059693	100.3176	3.2854	-1.8631	0.000633
64.2507	0.089485	101.8675	2.4094	-1.8478	0.000965
87.3001	0.121575	102.8724	1.8364	-1.8379	0.001345
133.3058	0.185626	104.1585	1.1728	-1.8255	0.002188
179.5855	0.250056	104.9528	0.7945	-1.8179	0.003177
264.0051	0.367585	105.8418	0.4142	-1.8095	
341.9293	0.47608	106.4304	0.2278	-1.8039	
400.9981	0.558324	106.7308	0.1405	-1.8011	
502.5147	0.699669	107.0232	0.0528	-1.7984	
593.6366	0.826541	107.2164	0.015	-1.7966	
644.4879	0.897343	107.3764	0.0049	-1.7951	
682.3278	0.950029	107.5547	0.0011	-1.7934	
705.9563	0.982928	107.8268	0.0001	-1.7909	

Table A.13: Sample A6002N: adsorption data for adsorbed nitrogen at 77K and calculated values when applying the equations DR and BET.

$P$ (mm Hg)	$\rho/\rho^o$	$V$ ( $cm^3$ CNPT $g^{-1}$ )	$A^2$ ( $kJ^2 mol^{-2}$ )	$\ln W$	$p/[V(\rho^o - \rho)]$
3.6821	0.005092	90.3008	3.3956	-1.9683	0.000057
6.8781	0.009522	95.1066	2.993	-1.9164	0.000101
24.1767	0.033521	101.8656	2.1837	-1.8478	0.00034
42.9373	0.059577	104.9325	1.8138	-1.8181	0.000604
68.9211	0.095631	106.5814	1.5095	-1.8025	0.000992
84.4684	0.117203	107.4024	1.3787	-1.7949	0.001236
129.5969	0.179861	108.8701	1.1033	-1.7813	0.002014
175.3022	0.243292	109.8641	0.909	-1.7722	0.002926
258.0301	0.358106	111.1348	0.6604	-1.7607	
327.6846	0.454776	112.0289	0.5067	-1.7527	
402.5622	0.558695	112.9003	0.3744	-1.7449	
506.9431	0.703561	113.7896	0.2261	-1.7371	
597.8213	0.829685	114.2738	0.1201	-1.7328	
658.3998	0.913758	114.6358	0.058	-1.7297	
682.9848	0.947879	114.9601	0.0344	-1.7269	
706.2513	0.980169	115.7609	0.0129	-1.7199	

Table A.14: Sample 6002N: mercury porosimetry data.

Pore radius (nm)	Accumulated volume ( $cm^3 g^{-1}$ )	Accumulated volume derivative ( $cm^3 g^{-1} nm^{-1}$ )
1807.82	0.002	0
319.34	0.043	0.000028
272.79	0.084	0.000881
240.23	0.128	0.001351
205.51	0.172	0.001267
154.58	0.212	0.000785
5.10	0.252	0.000268
2.14	0.252	0

Table A.15: Sample N6002: mercury porosimetry data.

Pore radius (nm)	Accumulated volume ( $cm^3 g^{-1}$ )	Accumulated volume derivative ( $cm^3 g^{-1} nm^{-1}$ )
1185.12	0	0
295.46	0.046	0.000052
265.33	0.088	0.001394
234.94	0.131	0.001415
198.99	0.173	0.001168
145.31	0.214	0.000764
2.44	0.254	0.00028
2.4	0.254	0

Table A.16: Sample A6002N: mercury porosimetry data.

Pore radius (nm)	Accumulated volume ( $cm^3 g^{-1}$ )	Accumulated volume derivative ( $cm^3 g^{-1} nm^{-1}$ )
1777.68	0	0
382.3	0.042	0.00003
323.22	0.087	0.000762
287.5	0.128	0.001148
251.56	0.173	0.001252
209.55	0.216	0.001024
142.4	0.257	0.000611
5.12	0.297	0.000291
2.66	0.297	0

Table A.17: Sample A6002N: carbon dioxide adsorption data at 273.15K and calculated values when applying the equations  $DR$ ,  $DA$  and  $S$ .

$P$ (mm Hg)	$\rho/\rho^o$	$V$ ( $cm^3$ CNPT $g^{-1}$ )	$A$ ( $kJ mol^{-1}$ )	$A^2$ ( $kJ^2 mol^{-2}$ )	$A^3$ ( $kJ^3 mol^{-3}$ )	$\ln W$
0.0525	0.000002	0.0514	29.8005	888.0688	26464.8797	-9.271
0.1034	0.000004	0.1036	28.2264	796.7278	22488.7321	-8.5701
0.1579	0.000006	0.1593	27.3056	745.5941	20358.8703	-8.1399
0.2104	0.000008	0.2111	26.6523	710.3425	18932.2273	-7.8583
0.3882	0.000015	0.4027	25.2247	636.2855	16050.1117	-7.2125
0.8274	0.000032	0.8446	23.504	552.4389	12984.5358	-6.4718
1.5754	0.00006	1.5119	22.0765	487.3705	10759.419	-5.8895
2.9334	0.000112	2.5595	20.659	426.7957	8817.186	-5.3631
4.5904	0.000176	3.6729	19.6326	385.4386	7567.1569	-5.0019
6.8141	0.000261	4.9531	18.7377	351.1031	6578.8798	-4.7029
16.1435	0.000618	9.1154	16.7802	281.5765	4724.922	-4.0929
23.1561	0.000886	11.5176	15.9622	254.791	4067.0182	-3.859
32.7234	0.001252	14.2273	15.1769	230.3388	3495.8329	-3.6477
44.4627	0.001701	16.9709	14.4809	209.6972	3036.6085	-3.4714
58.1672	0.002225	19.606	13.8711	192.4068	2668.8888	-3.3271
72.0785	0.002757	21.9012	13.3842	179.1371	2397.6092	-3.2164
88.2136	0.003374	24.1408	12.9256	167.0705	2159.4828	-3.119
103.5212	0.00396	25.9886	12.5619	157.8011	1982.2807	-3.0452
157.5634	0.006027	30.9472	11.6081	134.7473	1564.157	-2.8706
192.2124	0.007353	33.4744	11.1565	124.4668	1388.6103	-2.7921
216.2082	0.008271	35.0211	10.8893	118.5768	1291.2179	-2.7469
297.0336	0.011362	39.405	10.1682	103.3927	1051.3201	-2.629
399.331	0.015275	43.6704	9.4961	90.1767	856.3313	-2.5262
593.676	0.02271	49.3341	8.5955	73.8827	635.0591	-2.4043
687.0733	0.026282	51.4869	8.2638	68.2898	564.3308	-2.3616
740.08	0.02831	52.6509	8.095	65.5284	530.4498	-2.3392
791.9719	0.030295	53.6919				

Table A.18: Sample N6004: carbon dioxide adsorption data at 273.15K and calculated values when applying the equations *DR*, *DA* and *S*.

$P$ (mm Hg)	$\rho/\rho^o$	$V$ ( $cm^3$ CNPT $g^{-1}$ )	$A$ ( $kJ\ mol^{-1}$ )	$A^2$ ( $kJ^2\ mol^{-2}$ )	$A^3$ ( $kJ^3\ mol^{-3}$ )	$\ln W$
0.0645	0.000002	0.153	29.8005	888.0688	26464.8797	-8.1802
0.0837	0.000003	0.204	28.8797	834.0362	24086.7018	-7.8925
0.1072	0.000004	0.2548	28.2264	796.7278	22488.7321	-7.6702
0.1542	0.000006	0.3645	27.3056	745.5941	20358.8703	-7.3121
0.183	0.000007	0.4277	26.9555	726.5988	19585.8327	-7.1522
0.3817	0.000015	0.8922	25.2247	636.2855	16050.1117	-6.417
0.7999	0.000031	1.7378	23.5761	555.8334	13104.3957	-5.7503
1.5371	0.000059	3.0199	22.1146	489.0572	10815.3221	-5.1977
3.0978	0.000119	5.2459	20.5214	421.1261	8642.0788	-4.6454
4.4468	0.00017	6.8591	19.7114	388.5377	7658.6057	-4.3773
5.9473	0.000228	8.429	19.0447	362.7015	6907.5485	-4.1712
7.21	0.000276	9.7128	18.6108	346.3634	6446.1151	-4.0294
12.5142	0.000479	13.9206	17.3589	301.3299	5230.7431	-3.6695
17.3661	0.000664	17.0171	16.6172	276.1314	4588.53	-3.4687
18.9268	0.000724	17.9914	16.4207	269.6407	4427.7004	-3.413
29.4725	0.001127	23.1113	15.4158	237.6464	3663.5057	-3.1626
37.7307	0.001443	26.3815	14.8545	220.6556	3277.7239	-3.0302
53.9911	0.002065	31.5746	14.0406	197.1371	2767.9132	-2.8505
65.9876	0.002524	34.5716	13.5847	184.545	2506.9948	-2.7599
79.0194	0.003023	37.392	13.175	173.5817	2286.9459	-2.6814
104.155	0.003984	41.9958	12.5482	157.4566	1975.7918	-2.5653
152.8706	0.005848	48.691	11.6765	136.3416	1591.9986	-2.4174
173.711	0.006645	51.1632	11.3864	129.6499	1476.2445	-2.3679
203.5024	0.007785	54.3483	11.0268	121.5907	1340.7592	-2.3075
294.9314	0.011282	62.1165	10.1843	103.7193	1056.3052	-2.1739
395.1023	0.015114	68.4149	9.5202	90.6343	862.8577	-2.0773
593.46	0.022701	76.834	8.5964	73.8982	635.2587	-1.9612
699.8083	0.02677	80.2528	8.222	67.601	555.8145	-1.9177
736.2267	0.028163	81.4196	8.1068	65.7199	532.7774	-1.9033
791.6791	0.030284	82.9652	7.9419	63.0736	500.9233	-1.8845

Table A.19: Sample N6000: adsorption data for adsorbed nitrogen at 77K and calculated values when applying the equations *DR* and *BET*.

$P$ (mm Hg)	$\rho/\rho^o$	$V$ ( $cm^3$ CNPT $g^{-1}$ )	$A^2$ ( $kJ^2\ mol^{-2}$ )	$\ln W$	$p/[V(\rho^o - \rho)]$
3.7493	0.005176	81.4383	11.4585	-2.0716	0.000064
6.9402	0.00958	87.288	8.9349	-2.0022	0.000111
24.2285	0.033459	94.9922	4.7736	-1.9176	0.000364
44.5421	0.06159	98.4503	3.2129	-1.8819	0.000667
68.5844	0.094875	100.1815	2.294	-1.8645	0.001046
83.618	0.115697	100.9732	1.9238	-1.8566	0.001296
127.3327	0.176186	102.3295	1.2467	-1.8432	0.00209
169.2425	0.234175	103.2438	0.8715	-1.8343	0.002962
254.2258	0.351764	104.368	0.4514	-1.8235	
329.4608	0.455864	105.0431	0.2552	-1.8171	
403.8321	0.558769	105.5258	0.1401	-1.8125	
505.9899	0.700122	105.9496	0.0526	-1.8085	
598.808	0.828551	106.2495	0.0146	-1.8056	
649.4836	0.898669	106.4654	0.0047	-1.8036	
686.5684	0.949982	106.6979	0.0011	-1.8014	
710.7192	0.983399	107.0892	0.0001	-1.7978	

Table A.20: Sample N6004: adsorption data for adsorbed nitrogen at 77K and calculated values when applying the equations DR and BET.

$P$ (mm Hg)	$\rho/\rho^o$	$V$ ( $cm^3$ CNPT $g^{-1}$ )	$A^2$ ( $kJ^2 mol^{-2}$ )	$\ln W$	$p/[V(\rho^o - \rho)]$
3.751	0.005242	80.5269	11.4034	-2.0828	0.000065
6.859	0.009584	88.7916	8.9332	-1.9851	0.000109
24.7162	0.034505	97.5033	4.6875	-1.8916	0.000367
43.8301	0.061157	100.5763	3.2292	-1.8605	0.000648
66.7088	0.093044	101.9309	2.3321	-1.8471	0.001006
80.9718	0.112904	102.7468	1.9676	-1.8392	0.001239
118.8582	0.165681	103.9208	1.3365	-1.8278	0.001911
162.1902	0.226037	104.7578	0.9145	-1.8198	0.002788
248.5077	0.34628	105.5211	0.4651	-1.8125	
343.0841	0.478055	105.9704	0.2253	-1.8083	
416.4729	0.580316	106.1007	0.1225	-1.807	
517.7256	0.721402	106.0579	0.0441	-1.8075	
610.5128	0.850692	106.0917	0.0108	-1.8071	
660.2626	0.920014	106.1927	0.0029	-1.8062	
681.6727	0.949847	106.3931	0.0011	-1.8043	
707.2198	0.985444	106.6809	0.0001	-1.8016	

Table A.21: Sample N6000: mercury porosimetry data.

Pore radius (nm)	Accumulated volume ( $cm^3 g^{-1}$ )	Accumulated volume derivative ( $cm^3 g^{-1} nm^{-1}$ )
1006.24	0.008	0
355.54	0.049	0.000063
308.27	0.091	0.000905
274.19	0.134	0.001238
241.66	0.175	0.001267
198.62	0.216	0.000967
106.87	0.257	0.00044
2.13	0.257	0

Table A.22: Sample N6001: mercury porosimetry data.

Pore radius (nm)	Accumulated volume ( $cm^3 g^{-1}$ )	Accumulated volume derivative ( $cm^3 g^{-1} nm^{-1}$ )
1212.06	0.001	0
335.41	0.042	0.000046
288.27	0.086	0.000946
250.97	0.13	0.001164
216.35	0.172	0.001213
165.37	0.212	0.000792
5.31	0.252	0.00025
2.15	0.252	0

Table A.23: Sample N6003: mercury porosimetry data.

Pore radius (nm)	Accumulated volume ( $cm^3 g^{-1}$ )	Accumulated volume derivative ( $cm^3 g^{-1} nm^{-1}$ )
3555.37	0	0
478.30	0.04	0.000013
387.86	0.086	0.000509
325.19	0.128	0.00067
269.35	0.169	0.000734
186.80	0.209	0.000485
4.32	0.249	0.000219
2.89	0.249	0

Table A.24: Sample N6004: mercury porosimetry data.

Pore radius (nm)	Accumulated volume ( $cm^3 g^{-1}$ )	Accumulated volume derivative ( $cm^3 g^{-1} nm^{-1}$ )
1545.81	0	0
313.71	0.043	0.000035
267.32	0.088	0.00097
234.42	0.132	0.001337
193.93	0.174	0.001037
120.38	0.214	0.000544
2.69	0.214	0

Table A.25: Sample N4002: mercury porosimetry data.

Pore radius (nm)	Accumulated volume ( $cm^3 g^{-1}$ )	Accumulated volume derivative ( $cm^3 g^{-1} nm^{-1}$ )
1350.14	0.003	0
321.27	0.044	0.00004
274.19	0.087	0.000913
244.64	0.129	0.001421
214.61	0.171	0.001399
170.66	0.211	0.00091
19.38	0.252	0.000271
2.21	0.252	0

Table A.26: Sample N8002: mercury porosimetry data.

Pore radius (nm)	Accumulated volume ( $cm^3 g^{-1}$ )	Accumulated volume derivative ( $cm^3 g^{-1} nm^{-1}$ )
1269.77	0	0
293.83	0.043	0.000044
256.40	0.084	0.001095
225.50	0.125	0.001327
191.15	0.167	0.001223
136.40	0.207	0.000731
2.93	0.207	0

Table A.27: Sample N10002: mercury porosimetry data.

Pore radius (nm)	Accumulated volume ( $cm^3 g^{-1}$ )	Accumulated volume derivative ( $cm^3 g^{-1} nm^{-1}$ )
1640.94	0	0
272.09	0.043	0.000031
237.55	0.088	0.001303
207.92	0.131	0.001451
174.85	0.172	0.00124
115.31	0.212	0.000672
2.14	0.212	0